J Comput Neurosci (2011) 30:279–299
DOI 10.1007/s10827-010-0256-1

Can homeostatic plasticity in deafferented primary auditory cortex lead to travelling waves of excitation?

Michael Chrostowski · Le Yang · Hugh R. Wilson · Ian C. Bruce · Suzanna Becker

Received: 6 May 2009 / Revised: 6 June 2010 / Accepted: 18 June 2010 / Published online: 10 July 2010

Abstract Travelling waves of activity in neural circuits have been proposed as a mechanism underlying a variety of neurological disorders, including epileptic seizures, migraine auras and brain injury. The highly influential Wilson-Cowan cortical model describes the dynamics of a network of excitatory and inhibitory neurons. The Wilson-Cowan equations predict travelling waves of activity in rate-based models that have sufficiently reduced levels of lateral inhibition. Travelling waves of excitation may play a role in functional changes in the auditory cortex after hearing loss. We propose that down-regulation of lateral inhibition may be induced in deafferented cortex via homeostatic plasticity mechanisms. We use the Wilson-Cowan equations to construct a spiking model of the primary auditory cortex that includes a novel, mathematically formalized description of homeostatic plasticity. In our model, the homeostatic mechanisms respond to hearing loss by reducing inhibition and increasing excitation, producing conditions under which travelling waves of excitation can emerge. However, our model predicts that the presence of spontaneous activity prevents the development of long-range travelling waves of excitation. Rather, our simulations show short-duration excitatory waves that cancel each other out. We also describe changes in spontaneous firing, synchrony and tuning after simulated hearing loss. With the exception of shifts in characteristic frequency, changes after hearing loss were qualitatively the same as empirical findings. Finally, we discuss possible applications to tinnitus, the perception of sound without an external stimulus.

Keywords Primary auditory cortex · Peripheral hearing loss · Travelling wave · Homeostatic plasticity · Spiking neural model

Action Editor: S. A. Shamma

This research was supported by a New Emerging Teams Grant from the Canadian Institutes of Health Research to S.B. and I.B. and Discovery grants from the Natural Sciences and Engineering Research Council of Canada to S.B and I.B.

M. Chrostowski (✉)
McMaster Integrative Neuroscience Discovery & Study, McMaster University, 1280 Main Street West, Hamilton, ON, Canada, L8S 4K1
e-mail: chrostm@mcmaster.ca

L. Yang · I. C. Bruce
Department of Electrical and Computer Engineering, McMaster University, 1280 Main Street West, Hamilton, ON, Canada, L8S 4K1

H. R. Wilson
Center for Vision Research, York University, 4700 Keele Street, Toronto, ON, Canada, M3J 1P3

S. Becker
Department of Psychology, Neuroscience and Behaviour, McMaster University, 1280 Main Street West, Hamilton, ON, Canada, L8S 4K1

1 Introduction

Travelling waves of neuronal activity have been implicated in various various pathological conditions including brain injury (for a review, see Charles and Brennan 2009), migraine aura (Milner 1958) and epilepsy (Houweling et al. 2005). Potential mechanisms include transient hypoxia-induced changes in ion

balances (Takano et al. 2007) and long-term changes in the balance of excitation and inhibition. It has been proposed that such adaptations and the ensuing travelling waves may be a general feature of the brain's response to deafferentation (Houweling et al. 2005). In this paper we use a computational model of auditory cortex to explore the conditions under which travelling waves occur after sensory deafferentation, and the possibility that travelling waves may underlie some aspects of hearing loss including tinnitus.

The Wilson-Cowan equations (Wilson and Cowan 1972, 1973) describe the dynamics of a network of interconnected excitatory and inhibitory neurons. These equations predict the emergence of travelling waves of neural activity in the network when lateral inhibitory connections are sufficiently reduced. Travelling waves of activity have been implicated in cortical pathologies that involve deafferentation, such as epileptic seizures (Houweling et al. 2005). Cortical deafferentation also occurs with hearing loss and affects neural activity in the primary auditory cortex (Noreña and Eggermont 2003). However, no evidence of travelling waves has been found in the primary auditory cortex in animals with induced sensorineural hearing loss. We have developed a spiking model of the primary auditory cortex (A1), with excitatory and inhibitory neural units, in order to investigate the conditions required to induce travelling waves of neural activity after deafferentation. We propose a novel, well specified computational formalism for modeling homeostatic plasticity (HSP) within our detailed spiking cortical model as a mechanism to induce synaptic weight changes after deafferentation. The model allows us to shed light on the potential for travelling waves and other abnormal neural activity in A1 after sensorineural hearing loss.

Sensorineural hearing loss induced by aging and/or noise exposure is characterized by hair cell loss and some auditory nerve (AN) fiber damage (Bhattacharyya and Dayal 1989; Liberman 1987). The resulting distorted cochleotopic representation of the sound environment can cause profound changes in auditory brainstem (Brozoski et al. 2002; Kaltenbach et al. 2004), midbrain (Salvi et al. 2000; Wang et al. 2002) and cortex. At the level of primary auditory cortex, pyramidal neurons in the impaired region show increased neural synchrony and enhanced spontaneous activity within 2 hours after noise trauma (Noreña and Eggermont 2003). These cortical abnormalities persist in the weeks following noise exposure (Seki and Eggermont 2002, 2003). Moreover, after moderate to substantial cochlear damage, the tonotopic map is reorganized so that the neurons in the impaired region are re-tuned to respond maximally to frequencies near the edge of the hearing loss spectrum (Robertson and Irvine 1989; Rajan et al. 1993; Dietrich et al. 2001; Noreña et al. 2003). The mechanisms and timescale of the reorganization may depend on the severity of the peripheral damage (Noreña et al. 2003). An intriguing possibility is that the altered responsiveness of the cortex may set up the optimal conditions for travelling waves, which might in turn contribute to phenomena such as map reorganization and/or the phantom percept of tinnitus. We investigated whether travelling waves can propagate from regions representing edge frequencies of hearing loss into the deafferented region.

The underlying mechanisms for hearing loss-induced abnormal activities in A1 are still under investigation. An overall degradation of inhibition, possibly accompanied by the unmasking of excitatory synapses, may contribute to the observed cortical changes (Rajan 1998, 2001; Calford 2002; Noreña and Eggermont 2003). More recently, the compensatory effects of the reduced afferent drive in both auditory midbrain and A1 were discovered in animal experiments. In particular, the intrinsic excitability of the pyramidal neurons in the deafferented region of A1 is shown to be enhanced (Kotak et al. 2005). Moreover, the excitatory synapses targeted on the deafferented neurons are strengthened (Vale et al. 2002; Muly et al. 2004; Kotak et al. 2005) while the inhibitory synapses are weakened (Suneja et al. 1998a, b; Vale et al. 2002; Kotak et al. 2005). These synaptic regulations are consistent with homeostatic plasticity, previously observed in the hippocampus (Turrigiano et al. 1998) and the visual cortex (Desai et al. 2002).

We make the assumption that homeostatic mechanisms are at work in A1 after hearing loss and implement them in our model to scale both excitatory and inhibitory synapses on deafferented neurons. Homeostatic plasticity can ensure that, over a long timescale, the average neural firing rate can be maintained within a proper range, despite chronic changes in driving forces. Interestingly, the effects of homeostasis become detectable 1.5 hours after inducing persistent changes in neural activity and get stronger over a time-course of several days (Gina Turrigiano, personal communication). This timescale is similar to the temporal development of many of the cortical changes after noise trauma (Noreña and Eggermont 2003; Seki and Eggermont 2002, 2003). We propose that homeostatic mechanisms at work in the primary auditory cortex are at least partially responsible for abnormal activity that develops after hearing loss. Furthermore, by reducing lateral inhibitory weights and increasing lateral excitatory

weights, HSP is expected to produce conditions that increase the potential for travelling waves.

Recent theoretical models of hearing loss in the auditory brainstem (Schaette and Kempter 2006) and A1 (Dominguez et al. 2006) provide insights into the possible contributions of HSP to tinnitus, but have not included a sufficient level of biological detail to implement realistic temporal dynamics in neural circuits so as to be able to investigate travelling waves.

Using a comprehensive description of HSP, we can make predictions about conditions required for travelling waves of neural activity. We look at changes in sound-driven and spontaneous activity, along with tuning properties in the auditory cortex, in the hours after hearing loss to determine if our model can reproduce findings in animal models of sensorineural hearing loss. We then investigate the potential for travelling waves. We assume that, during this period of time, changes in cortical activity are dominated by altered thalamic input rates and homeostatic mechanisms within the auditory cortex responding to the altered input. Compared to the previous work by Dominguez et al. (2006), this A1 model is able to better capture the altered cortical activity and changes in neural tuning. Changes in neural activity and tuning sharpness are qualitatively similar to empirical findings. We do not see meaningful shifts in characteristic frequencies after simulated hearing loss. Homeostatic plasticity in our model (and perhaps *in vivo*) may not be a sufficient mechanism for tonotopic reorganization. Furthermore, we do not include peripheral or subcortical changes that would contribute to these shifts. Rather, we focus on alterations in cortical connections and activity.

Surprisingly, our simulations show that travelling waves of excitation with large temporal extent do not manifest as predicted in a spiking model with spontaneous firing. The waves of excitation are prevented from traversing the network by refractory periods produced by spontaneous firing. In the biologically unlikely scenario where there is no spontaneous firing, travelling waves emerge as predicted. While the effect of decreased inhibition is to increase the likelihood of travelling waves, this is offset by the HSP-induced increase in spontaneous firing. However, our model demonstrates that shorter-duration spontaneous travelling waves of excitation become more frequent and span large portions of the hearing loss region. This prediction may be important in explaining the lack of empirical evidence for travelling waves of activity in A1 after sensorineural hearing loss.

2 Spiking A1 model

In this section, the development of our spiking A1 model is presented in detail. In particular, we first describe the network architecture. Then, the model neuron and the input to the A1 model are illustrated. Finally, a novel formulation for the computational principles underlying HSP in different types of synapses is presented.

2.1 Network model

The network is designed based on several key features of A1 observed in animal experiments and neuroimaging studies in humans. First, when stimulated with pure-tone stimuli with varying sound pressure levels (SPL), many A1 pyramidal neurons exhibit a V/U-shaped tuning curve with a single best frequency or characteristic frequency (CF) (Phillips and Irvine 1981; Schreiner et al. 2000; Turner et al. 2005). The CF is usually defined as the frequency with the lowest response threshold. Second, in normal hearing animals and humans, the CFs of the pyramidal neurons show a roughly one-dimensional gradient along the latero-medial axis, and they display a logarithmic relation to the corresponding cortical locations. This property is known as the tonotopic organization of A1 or simply referred to as the tonotopic map (Merzenich et al. 1975; Cheung et al. 2001; Ottaviani et al. 1997). Third, the interneuron population in A1 provides inhibitory inputs that are thought to sharpen the receptive fields of the pyramidal neurons (Chen and Jen 2000; Foeller et al. 2001), a mechanism also observed in subcortical auditory structures such as IC (Gerken 1996; Lu and Jen 2001). Finally, the excitatory connections between pyramidal neurons in the direction of the lateral-medial axis are generally short-range, while lateral connections between pyramidal neurons and inhibitory interneurons span a broader region (Douglas and Martin 1998). For a more comprehensive description of A1 anatomy and functional organization, see Read et al. (2002) and references therein.

With the above observations in mind, we construct the A1 model by modifying the well-known Wilson-Cowan cortical model (Wilson and Cowan 1972, 1973). A schematic diagram of the network structure is given in Fig. 1. Our A1 model is driven by a set of model neurons representing the afferent inputs from the auditory thalamus. In the cortical layer, pyramidal neurons are uniformly distributed along the latero-medial axis connecting the posterior ectosylvian suclus and anterior ectosylvian suclus. There are 201 pyramidal neurons and 67 interneurons, which is consistent with

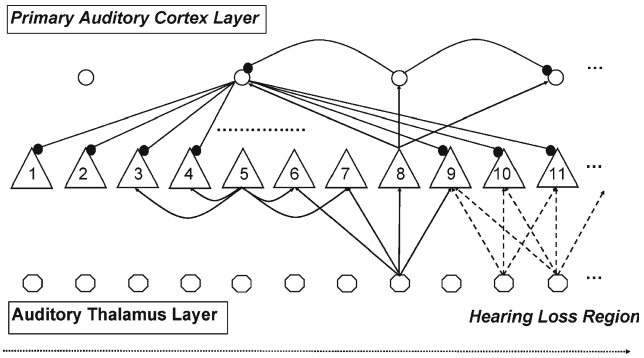

Fig. 1 The schematic structure of the spiking A1 model. The numbered triangles represent pyramidal neurons. The associated digit denotes the spatial coordinate of the given neuron. Inhibitory interneurons and thalamic neurons are represented by open circles and regular octagons, respectively. Arrowed lines are excitatory synapses, while lines ending with full black circles denote inhibitory synapses. Hearing loss is illustrated by using dashed lines for afferent synapses to show the reduction in inputs

the finding that typically around 75% of cortical cells are glutamatergic neurons while the rest are inhibitory neurons (Jones 1995). The number of neurons and connections in our computational model is a subset of what one would find in the auditory cortex, however, it was necessary to make the simulations computationally viable while maintaining the validity of the model and results. We associate each pyramidal neuron with a one-dimensional coordinate x_i such that $x_i = i$, $i = 1, 2, 3, ..., 201$. Note that in contrast to many existing spiking models for auditory midbrain (e.g., Bruce et al. 2003) and A1 (e.g., Dominguez et al. 2006), inhibitory interneurons are separately incorporated in the present model. To facilitate the initialization of the synaptic weight matrices, we organize the interneurons on a straight line parallel to the latero-medial axis. It is assumed that the interneurons are equally spaced with a distance three times larger than that between two pyramidal neurons, as shown in Fig. 1. Therefore, the spatial coordinates for the interneurons y_j are given by $y_j = 3(j-1)+2$, $j = 1, 2, 3, ..., 67$. There are 201 neurons in the auditory thalamus layer. Their spatial coordinates are denoted by z_k, where $z_k = k$, $k = 1, 2, 3, ..., 201$. The CFs of thalamic neurons range from 20 Hz to 20 kHz and correspond to the approximately logarithmic dependence between CF and position on the basilar membrane (Greenwood 1990).

The synapses in the A1 model are initialized under simulated normal hearing conditions, where a pyramidal neuron has the same characteristic frequency as a thalamic neuron when they share the same spatial coordinate. We then simulate hearing loss and a subsequent period of adaptation of the network response to acoustic inputs, during which time the synaptic weights are modified by a set of HSP rules (derived in Section 2.4). The resultant changes in synaptic efficacy can potentially cause shifts in the CFs of pyramidal neurons, i.e., cortical reorganization, while the CFs of thalamic neurons remain fixed.

Based on experimental data (Miller et al. 2001), we require that for normal hearing, a pyramidal neuron is driven by thalamic neurons whose CFs lie in the range of $\pm 1/3$ octaves of the pyramidal neuron's characteristic frequency, through excitatory thalamocortical synapses. When simulating synaptic modifications by HSP in hearing loss scenarios, we assume that pyramidal neurons continue to receive afferent inputs solely from those thalamocortical synapses, i.e., we do not consider any unmasked thalamocortical synapses in this model. In this way, we can investigate the contribution of HSP to the observed cortical changes separately (see more in *Discussion*). The synaptic strength of the afferent connection from the kth thalamic neuron to the ith pyramidal neuron, denoted by $\mathbf{W_a}(i,k)$, is determined by the following Gaussian function[1]:

$$\mathbf{W_a}(i,k) = \begin{cases} 0.3 \cdot \exp\left(-\dfrac{|z_k - x_i|^2}{3.684}\right), & |z_k - x_i| \le 9 \\ 0, & |z_k - x_i| > 9 \end{cases} \tag{1}$$

Pyramidal neurons are also depolarized through lateral excitatory synapses. These connections are assumed to span a range of $\pm 1/6$ octaves with the efficacy of the synapse from the lth pyramidal neuron to the ith one $\mathbf{W_{E,E}}(i,l)$ also falling off as a Gaussian function of distance:

$$\mathbf{W_{E,E}}(i,l) = \begin{cases} 0.21 \cdot \exp\left(-\dfrac{|x_i - x_l|^2}{6.72}\right), \\ |x_i - x_l| \le 5 \text{ and } x_i \ne x_l \\ 0, \\ |x_i - x_l| > 5 \text{ or } x_i = x_l \end{cases} \tag{2}$$

where $l = 1, 2, 3, .., 201$. From the above equation, it can be seen that we do not assume direct self-excitation in our model.

The interneurons in the A1 layer are driven by the output spikes of pyramidal neurons and then feed inhibition back to sharpen frequency tuning. The synaptic weight of the lateral connection from the ith pyramidal

[1] The peak values and variances of the Gaussian functions defined in this subsection are chosen so that a tonal stimulus would only excite a small portion of the pyramidal neurons. See the model response to a 723-Hz pure tone in Fig. 8 for an example.

neuron to the jth interneuron, denoted by $\mathbf{W_{I,E}}(j,i)$, is expressed as

$$\mathbf{W_{I,E}}(j,i) = \begin{cases} 0.11 \cdot \exp\left(-\dfrac{|x_i - y_j|^2}{41.5}\right), & |x_i - y_j| \le 20 \\ 0, & |x_i - y_j| > 20 \end{cases} \tag{3}$$

The efficacy of the feedback inhibitory synapse from the jth interneuron to the ith pyramidal neuron $\mathbf{W_{E,I}}(i,j)$ is determined by

$$\mathbf{W_{E,I}}(i,j) = \begin{cases} 0.4 \cdot \exp\left(-\dfrac{|x_i - y_j|^2}{41.5}\right), & |x_i - y_j| \le 20 \\ 0, & |x_i - y_j| > 20 \end{cases} \tag{4}$$

In comparison to the pyramidal neurons, the inhibitory interneurons receive lateral excitatory inputs from a wider range of pyramidal neurons, spanning about ±3/4 octaves. Moreover, as shown in (4), feedback inhibition from an interneuron imposes mutual competition between those pyramidal neurons that drive the interneuron to form a lateral inhibitory network.

We also include lateral inhibitory synapses among interneurons. Their synaptic weights are given by

$$\mathbf{W_{I,I}}(j,m) = \begin{cases} 0.048 \cdot \exp\left(-\dfrac{|y_j - y_m|^2}{220}\right), \\ |y_j - y_m| \le 9 \text{ and} y_j \ne y_m \\ 0, \\ |y_j - y_m| > 9 \text{ or } y_j = y_m \end{cases} \tag{5}$$

where $m = 1, 2, 3, ..., 67$. We set the lateral inhibition between interneurons to be small in order to avoid broadening the tuning curves of the pyramidal neurons. And again, there is no self-inhibition. It is worthwhile to point out that as in the previous modeling work (Dominguez et al. 2006), we do not incorporate either corticofugal projections from A1 onto the auditory thalamus or the feed-forward inhibition from thalamic neurons to pyramidal cells via cortical interneurons. Corticothalamic feedback projections may play a role in enhancing tuning curves, but they have not been characterized sufficiently to be included in our model. Feed-forward inhibition may likely be an important mechanism for improving temporal precision of auditory responses. Furthermore, co-tuned inhibition may sharpen tuning curves of cortical neurons while convergence of thalamocortical inputs may be the main contributor to the shape of these tuning curves as has been proposed by Wehr and Zador (2003). However, homeostatic plasticity may alter both the thalamocortical and intracortical connections described above, affecting tuning in A1. Therefore, our model's architecture can provide insights into potential effects of a homeostatic plasticity mechanism on activity in A1.

To reduce network edge effects, appropriate weight adjustments of the synapses targeted on cortical neurons near/at the edge of the A1 layer are performed to match the total excitation/inhibition for neurons in the middle sections. As neurons at or near the array edge can be considered to be missing lateral inputs from one side (tonotopically), this is adjusted for by increasing their existing excitatory and inhibitory connection weights until their total excitation and inhibition are equal to that of a neuron with all of its inputs (as in Bruce et al. 2003). As the start of the hearing loss region is modeled at a sufficient distance from the end of the array of neural units, this compensatory measure will not have an impact on the findings discussed in this paper.

2.2 Model neuron

In this work, both pyramidal neurons and interneurons are modeled as leaky integrate-and-fire neurons (e.g., Gerstner and Kistler 2002). Specifically, when the membrane potential of a cortical neuron reaches a certain threshold, the neuron fires a spike and enters an absolute refractory period of 2 milliseconds (ms). During that period, the membrane potential is fixed at the resting potential and allowed to vary again thereafter. Note that we do not include the relative refractory period in the neuron model for simplicity. The sub-threshold behaviors of the pyramidal neurons and interneurons are governed by

$$\tau \frac{d\mathbf{V_E}(t)}{dt} = -\mathbf{V_E}(t) + \mathbf{W_{E,E}} \cdot \mathbf{i_E}(t) - \mathbf{W_{E,I}} \cdot \mathbf{i_I}(t) + \mathbf{W_a} \cdot \mathbf{i_a}(t), \tag{6}$$

and

$$\tau \frac{d\mathbf{V_I}(t)}{dt} = -\mathbf{V_I}(t) + \mathbf{W_{I,E}} \cdot \mathbf{i_E}(t) - \mathbf{W_{I,I}} \cdot \mathbf{i_I}(t), \tag{7}$$

respectively. The connection weight matrices $\mathbf{W_a}$, $\mathbf{W_{E,E}}$, $\mathbf{W_{I,E}}$, $\mathbf{W_{E,I}}$ and $\mathbf{W_{I,I}}$ have been defined in the last subsection. $\mathbf{V_E}(t)$ is a column vector of length 201 containing the membrane potentials of the pyramidal

neurons. $\mathbf{V_I}(t)$ denotes a column vector representing the membrane potentials of the interneurons. τ (=2.75 ms) is the membrane time constant. $\mathbf{i_a}(t)$ and $\mathbf{i_E}(t)$ are column vectors of length 201 describing the afferent and lateral excitatory synaptic currents from the thalamic neurons and pyramidal neurons, respectively. $\mathbf{i_I}(t)$ is the column vector of length 67 describing the inhibitory synaptic currents from the interneurons at time t. Each synaptic current is obtained by convolving the corresponding spike train with a unitary postsynaptic current waveform

$$i(t) = \left(\frac{a}{10\tau}\right)^2 \cdot \exp(-at/\tau) \cdot t, \tag{8}$$

which is commonly referred to as the alpha function (see Dayan and Abbott 2005). Excitatory synaptic currents are generated using an alpha function with $a = 10$, while inhibitory synaptic currents are calculated with $a = 0.5$.

2.3 Model input

We simulate three different input scenarios: one in which the model is stimulated by a simplified acoustic environment, one in which the model is situated in a quiet background, and a simulated pure tone input, which we use to demonstrate changes in network dynamics after hearing loss. For the first scenario, the input consists of the response of the subcortical auditory pathway to sound stimuli, while in the second scenario, the input consists of the afferent spontaneous activity from the auditory midbrain. A real-life acoustically rich environment is a constantly changing mixture of sounds of all frequencies. We approximate this situation using a simplified acoustic environment where the power spectrum of the sound stimuli over the range 20 Hz to 20 kHz is flat and there is no correlation between different frequency components. Accordingly, the spike trains generated by thalamic neurons in response to acoustic inputs are modeled as mutually independent Poisson processes. The sound-driven mean rates of the thalamic neurons' spike trains across the tonotopic map are set to be 150 spikes per second in the case of normal hearing. This input rate is high enough to be delineated from the silent condition and for sufficiently separable simulation results for the three hearing loss conditions we describe below. Furthermore, because the model has a lower density of neurons than real A1 due to computational limitations, having a higher input rate approximates the case of having a larger number of inputs with lower discharge rates. Using input rates that are this high does not qualitatively affect our results, but does lead to mean firing rate in the pyramidal neurons that are higher than what would be found in electrophysiological recordings. Using a uniform input rate for the simplified acoustic environment does not capture the various driving rates that would result from a dynamic acoustically rich-environment, however it does make the simulation of hearing loss curves and effects of the homeostatic mechanism clearer. A benefit of the mutually independent thalamocortical inputs is that it allows us to isolate the effect of hearing loss on cortical synchrony. However, in future work, it will be worthwhile to simulate more dynamic and complex acoustic environments in order to determine how inputs with a more natural spectro-temporal structure affect network activity.

After cochlear damage, it has been observed experimentally that the auditory brainstem response threshold increases and the auditory nerve output decreases (Salvi et al. 1980). Thus, we model the effects of peripheral hearing loss by reducing the sound-driven average rates of the spike trains of thalamic neurons at the impaired frequencies. We simulate a large normal hearing region, a transition region, and a large impaired region to facilitate the analysis and presentation of our results. Auditory peripheral damage mainly affects the processing of high-frequency components of the sound stimuli, because the hair cells tuned to those frequencies are especially vulnerable to noise trauma as well as age-related degeneration. Therefore, we constrain the mean spike rate decrease to the output spike trains of thalamic neurons with relatively high CFs. We define the hearing loss severity as the ratio of the maximum rate reduction to the normal sound-driven thalamic spike rate (=150 spikes/s). In this study, we consider three different hearing loss levels, specifically, 40%, 60% and 80%. Due to the existence of inputs from horizontal fibers and other cortico-cortical synapses, an 80% loss in driving spikes to A1 neurons is less likely to occur in standard animal models of noise-induced hearing impairment. However, we include the simulation results for 80% hearing loss in order to better illustrate the effects of HSP on synaptic weights and cortical activity across a broad range of deafferentation levels. Furthermore, the 80% hearing loss case allows us to more strongly demonstrate our findings related to travelling waves of excitation in the presence of spontaneous firing. For all three hearing-loss scenarios, hearing loss starts at 2.5 kHz, and its severity increases as a linear function of the spatial coordinates of the thalamic neurons until it reaches the maximum at 5 kHz. For the frequency range from 5 kHz to 20 kHz, the amount of hearing loss is the same as that at 5 kHz. As an example,

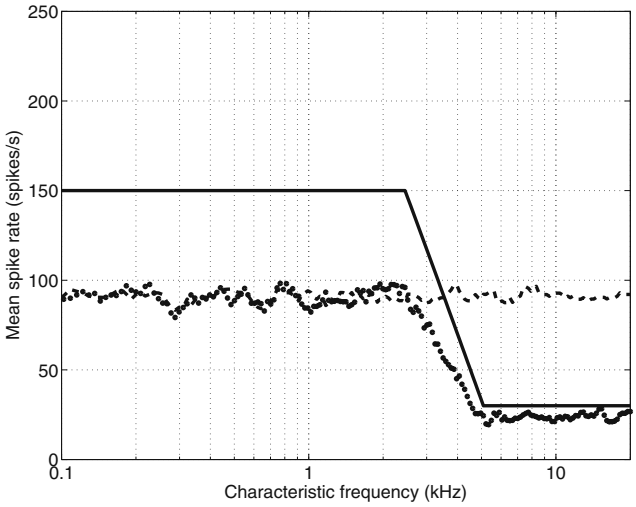

Fig. 2 Mean firing rates of the pyramidal neurons after 80% hearing loss (mean spike rate vs. characteristic frequency). Solid line: hearing loss curve; dotted line: the A1 model without HSP; dashed line: the A1 model with HSP. Note that in this figure and the following Figs. 4 and 6, the values on the x-axis denote the characteristic frequencies that the pyramidal neurons are tuned to under the condition of normal hearing. In other words, they indeed represent the spatial coordinates of the pyramidal neurons

Fig. 2 shows the mean firing rate curve for the 80% hearing loss case, which has a maximum rate reduction of 120 spikes/s. Qualitatively similar hearing loss curves illustrated by the auditory brainstem response (ABR) shift have been induced in cats (Noreña and Eggermont 2003) via excessive noise exposure. More recent audiogram data from humans with noise-induced hearing loss also exhibit similar hearing loss curves (Konig et al. 2006).

When the A1 model is situated in a quiet background, the driving force is the afferent spontaneous activity again modeled as mutually independent Possion spike trains. But in this case, we assume that the mean spike rate is 5 spikes/s across the whole frequency range, regardless of the hearing loss level. This setting is mainly motivated by *in vivo* experiments showing that most neurons in the auditory midbrain have similar spontaneous rates and their spontaneous activities remain largely unchanged after cochlear damage (Wang et al. 1996).

We test the A1 model initialized in the last subsection under two different input scenarios described above: the simplified acoustic environment and the silent condition. For both input scenarios, we simulate the condition of normal hearing in order to estimate mean firing rates of pyramidal neurons in the normal model. We use the pure-tone input condition to test for travelling waves of activity in the hearing loss conditions. The induced thalamic response resulting from a pure tone, $\mathbf{y_{pt}}(i,k)$ centered at neural unit z_k, and with peak amplitude A, is modeled as an increase in spike rate falling off spatially as a Gaussian:

$$\mathbf{y_{pt}}(k) = \begin{cases} A \cdot \exp\left(-\dfrac{|z_k - x_i|^2}{12.5}\right), & |z_k - x_i| \le 9 \\ 0, & |z_k - x_i| > 9 \end{cases} \quad (9)$$

The model operation is simulated using a 4^{th}-order Runge-Kutta algorithm with a fixed time-step of 0.1 milliseconds.

2.4 Homeostatic plasticity

Homeostatic plasticity (HSP) is triggered in response to the deviation of neural activity from a prefixed target rate (r_{target}) and its compensatory effects can bring the average firing rate back to normal (Burrone and Murthy 2003). As shown in animal experiments (Turrigiano et al. 1998; Kilman et al. 2002), HSP operates in a multiplicative fashion, i.e., all synaptic weights are enhanced or suppressed by the same scaling factor. In this way, HSP can stabilize neural activity without distorting the original synaptic distribution. Moreover, it has been observed that HSP regulates the synaptic efficacy slowly but accumulatively (Turrigiano et al. 1998; Desai et al. 2002). van Rossum et al. (2000) proposed a framework for implementing the homeostatic regulation of excitatory synapses targeted on spiking neurons that captures the key features of HSP mentioned above. Based on recent experimental studies on HSP, we extend the modeling work by van Rossum et al. to formulate a set of computational principles of HSP for synapses of different types in our A1 model.

Deafferentation can lead to the scaling-up of the synaptic efficacy of the thalamocortical synapses (Kotak et al. 2005) and the lateral excitatory synapses (Turrigiano et al. 1998; Rutherford et al. 1998; Kotak et al. 2005), while hyperactivity of the pyramidal neurons could lead to multiplicative depression (Turrigiano et al. 1998; Leslie et al. 2001). As such, similar to the realization of HSP for excitatory synapses developed by van Rossum et al. (2000), we use the following equations to update the matrices $\mathbf{W_a}$ and $\mathbf{W_{E,E}}$:

$$\tau_{\mathrm{HSP}} \frac{\mathrm{d}\mathbf{W_a}(i,k)}{\mathrm{d}t} = \big(r_{target} - r_i(t)\big) \cdot \mathbf{W_a}(i,k), \quad (10)$$

and

$$\tau_{\mathrm{HSP}} \frac{\mathrm{d}\mathbf{W_{E,E}}(i,l)}{\mathrm{d}t} = \big(r_{target} - r_i(t)\big) \cdot \mathbf{W_{E,E}}(i,l), \quad (11)$$

where $i = 1, 2, 3, ..., 201$, $k = 1, 2, 3, ..., 201$ and $l = 1, 2, 3, ...201$. The time constant τ_{HSP} is set to be 10^4 s (approximately 2.8 hours). The mechanism underlying the time constant of homeostatic plasticity is not clear, so we assume all cortical neurons have the same HSP time constant. The instantaneous firing rate of the ith pyramidal neuron $r_i(t)$, where $i = 1, 2, 3, ..., 201$, is defined as (van Rossum et al. 2000)

$$\tau_r \frac{\mathrm{d}r_i(t)}{\mathrm{d}t} = -r_i(t) + \sum_n \delta(t - t_{n,i}) \tag{12}$$

where τ_r is set to be 1s, $t_{n,i}$ is the time point of the nth spike generated by the ith neuron, and $\delta(x)$ denotes the Dirac delta function. It can be seen from the above equation that $r_i(t)$ increases whenever the neuron fires a spike, and it decreases exponentially between spikes. The value of r_{target} is selected in order to represent the mean firing rate of pyramidal neurons in response to acoustic stimuli under the condition of normal hearing. In our simplified acoustic environment, pyramidal neurons in the cortical layer have mean firing rates around 90 spikes/s, therefore, we use this value for r_{target}. We used a target rate that is higher than the normal spontaneous firing rate of the A1 model in a completely quiet background (=2.5 spikes/s) because humans are generally exposed to acoustic environments that may induce a higher average rate of cortical firing. Furthermore, sensorineural hearing loss has been shown to induce a persistent increase in spontaneous firing of cortical neurons (Seki and Eggermont 2003). This may be partly due to a homeostatic set point for pyramidal neurons in the primary auditory cortex that is above the normal spontaneous firing rate. The purpose of a target firing rate and a homeostatic drive towards it could be to optimize information processing of relevant auditory stimuli (see Parra and Pearlmutter (2007) for a discussion of the optimality of gain adaptation mechanisms).

Compared with the excitatory synapses targeted on pyramidal neurons, our proposed mechanism for HSP adjusts the feedback inhibitory synapses in an opposite direction, consistent with empirical findings by Turrigiano and colleagues (Rutherford et al. 1997; Kilman et al. 2002; Kotak et al. 2005). In other words, hyperactivity of pyramidal neurons would enhance inhibitory neurotransmission while deafferentation induced by hearing loss would reduce the efficacy of the inhibitory synapses. Therefore, building on Eqs. (10) and (11), we develop the following equation to modify the entries in $\mathbf{W_{E,I}}$:

$$\tau_{\text{HSP}} \frac{\mathrm{d}\mathbf{W_{E,I}}(i,\, j)}{\mathrm{d}t} = -\left(r_{target} - r_i(t)\right) \cdot \mathbf{W_{E,I}}(i,\, j), \tag{13}$$

where $j = 1, 2, 3, ..., 67$. The homeostatic regulation of the matrix $\mathbf{W_{I,E}}$ is a bit more complex. Experiments show that activity blockade does not influence the lateral connections from pyramidal neurons onto interneurons (Turrigiano et al. 1998; Rutherford et al. 1998), while hyperactivity does increase their efficacy (Rutherford et al. 1998). A hyperactivity threshold for regulating pyramidal projections onto interneurons takes these findings into account and prevents the HSP mechanism from acting on the connections unless the threshold is exceeded. Thus, we formulate the updating equation for $\mathbf{W_{I,E}}$ as follows

$$\tau_{\text{HSP}} \frac{\mathrm{d}\mathbf{W_{I,E}}(j, i)}{\mathrm{d}t} = -\left(r_{target} - r_i(t)\right) \cdot u(-\left(r_{target} - r_i(t)\right) - h) \cdot \mathbf{W_{I,E}}(j, i), \tag{14}$$

where $u(x)$ is the unit-step function, that is, $u(x) = 1$ if $x \geq 0$; otherwise, $u(x) = 0$. h is the prefixed threshold for gating the hyperactivity, which is set to be 10 spikes/s. To our knowledge, there is no evidence on the homeostatic regulation for lateral inhibitory connections between interneurons. As such, we simply fix them during computer simulations.

For our model we have set τ_{HSP} so that HSP acts on a timescale of hours, consistent with some empirical findings (Gina Turrigiano, personal communication). However, homeostatic plasticity in the adult visual system of a goldfish with an intact CNS was found to operate on a timescale of 90 minutes (Riegle and Meyer 2007). HSP mechanisms acting on a shorter timescale than what is implemented in our model may be feasible but require further investigation.

At this point, the specification of the spiking A1 model with homeostatic plasticity is complete and the operations of the homeostatic mechanisms and model behavior after hearing loss are simulated.

3 Results

In this section, we investigate the performance of the model through computer simulations. Specifically, the model is first trained under different hearing loss scenarios for a sufficiently long time period so that the sound-driven firing activity of the pyramidal neurons can reach equilibrium under the control of HSP. For all three hearing loss scenarios, we observe that homeostatic plasticity is able to compensate for the deafferentation and maintain the mean sound-driven neural firing rate of the pyramidal neurons in

a small region around the pre-fixed target value r_{target} (=90 spikes/s). Figure 2 shows comparative curves representing the average firing rates of the pyramidal neurons with and without HSP in the case of 80% hearing loss. It can be seen that with HSP, the average firing rate curve is relatively flat around 90 spikes/s, while the average firing rate curve generated by the A1 model without HSP exhibits a negative slope similar to the hearing loss curve. In Fig. 3, we plot the connection weights of synapses targeting on two pyramidal neurons, one in the normal hearing region and the other in the mid-section of the most substantially deafferentated region. With HSP, the shape of the weight distribution for synapses targeted on the impaired neuron is not changed. This is because the afferent and lateral excitatory connections are strengthened in a multiplicative fashion, and the feedback inhibitory synapses are weakened by the same factor. The excitatory connections on the interneurons are not affected by our HSP mechanism, as explained above. More importantly, the weight envelopes in Fig. 3 describing the peak synaptic weight for neurons across the tonotopic axis, show that the amount of synaptic adjustment induced by HSP is a function of the hearing loss level; a sufficient level of hearing loss in our model should therefore lead to conditions that are favourable to travelling waves. The more severe the hearing loss, the greater compensatory effects and the higher the excitability of the pyramidal neurons would be, which is consistent with experimental results on homeostatic plasticity (Turrigiano et al. 1998; Rutherford et al. 1998; Kilman et al. 2002). This also holds for inhibitory connection weights, which are reduced in proportion to the level of deafferentation. Because our HSP mechanism scales synapses multiplicatively, the ratio of afferent to lateral excitation remains fairly constant. On the other hand, the ratio of lateral inhibition to lateral excitation on pyramidal cells drops as the level of hearing loss increases; this may

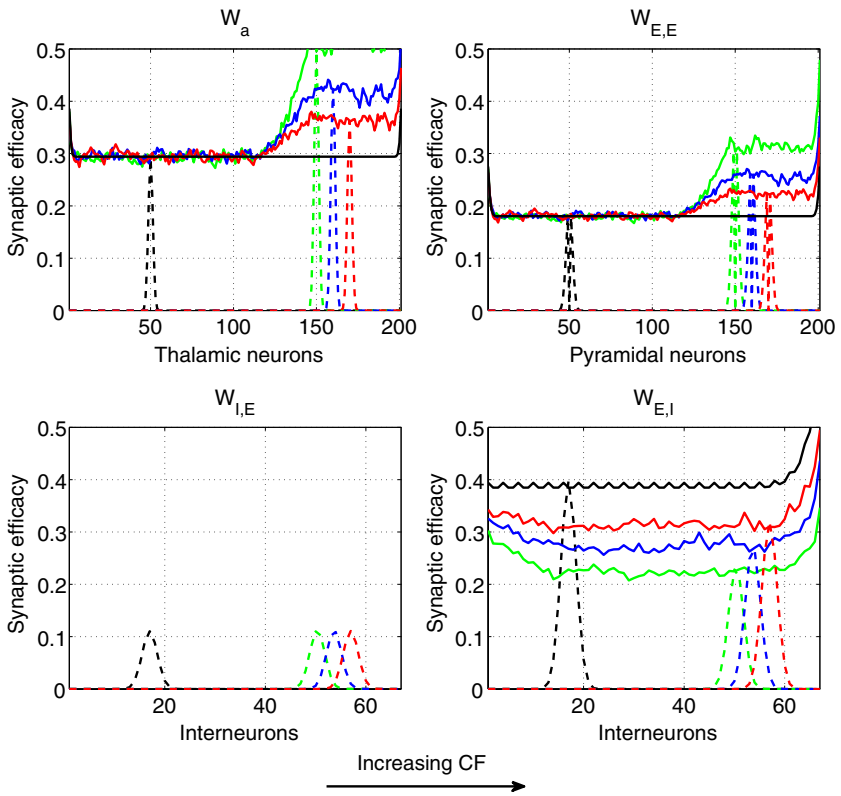

Fig. 3 Connection weight distribution comparison after HSP. Dashed lines show example weight distributions for synapses targeted on the 50th pyramidal neuron (CF=0.37 kHz) and a pyramidal neuron in the deepest hearing loss region for each hearing loss level. Solid curves represent peak synaptic efficacy in weight distributions for each neuron (shown only for synapses projecting onto excitatory neurons). Black curve: Unimpaired neurons with synapses unaffected by HSP (initial weights are all at this level except for weights at edges). Green curve: synapses targeted on the 150^{th} pyramidal neuron (CF=5.76 kHz) after 80% hearing loss; Blue curve: synapses targeted on the 160^{th} pyramidal neuron (CF=7.34 kHz) after 60% hearing loss; Red curve: synapses targeted on the 170^{th} pyramidal neuron (CF=9.41 kHz) after 40% hearing loss. sub-figure $\mathbf{W_a}$: weight comparison for thalamocortical afferent synapses; sub-figure $\mathbf{W_{E,E}}$: weight comparison for lateral excitatory synapses; sub-figure $\mathbf{W_{I,E}}$: weight comparison for synapses projecting onto interneurons; sub-figure $\mathbf{W_{E,I}}$: weight comparison for feedback inhibitory synapses

have implications for the development of travelling waves, as will be discussed later.

The inputs to the model are independent and do not take into account potential HSP-induced changes in lateral inhibitory connections in lower auditory structures such as the inferior colliculus (Gerken 1996). This allows us to consider changes in the auditory cortex independent of confounding factors in the inputs. However, we acknowledge that future versions of the model should address potential changes at subcortical levels to determine their effect on our simulations.

Next, we fix the synaptic weights and expose the model to afferent spontaneous activity or transient tonal stimuli. We present the obtained model responses in the following subsections. The first two sections are meant to validate the model by comparing its simulations to empirical findings. In the following section, we evaluate the robustness of our model with respect to two key validating results. Finally, we outline simulations related to our novel prediction on the existence of travelling waves of excitation in A1.

3.1 Spontaneous activity and synchrony

In Fig. 4, we plot the mean firing rates of the pyramidal neurons in the A1 layer in response to the afferent spontaneous activity from the auditory thalamus. The results presented here are calculated on the basis of a simulated 30-second recording. As we can see from the figure, for all three hearing loss scenarios, the impaired region of the A1 model shows a significant increase in its spontaneous activity, which is qualitatively consistent with empirical findings in animals with noise-induced hearing loss (Popelar et al. 1994; Komiya and Eggermont 2000; Seki and Eggermont 2003). Furthermore, the input-output plot in the figure shows that when a deafferented neuron is driven by tonal stimuli of different intensities, the neuron consistently has a greater level of excitability than an unimpaired neuron for a given input spike rate. Spontaneous activity in the impaired region for 60% hearing loss is around two to three times higher than that for 40% hearing loss. Increase in spontaneous firing rate in the case of 80% hearing loss is even more significant (around five times higher than that of 40%). This is due to the fact that more substantial hearing loss results in greater enhancement in the excitability of pyramidal neurons, as observed in the previous section. In animal experiments, the enhanced spontaneous activity in the impaired cortical region is no higher than double the normal value (Komiya and Eggermont 2000; Seki and Eggermont 2003). Our results showing a much higher increase in spontaneous firing rate in the case of 80% hearing loss can be attributed to the substantially reduced afferent driving forces, which is less likely to be observed in standard animal models, as mentioned earlier. However, this qualitatively valid result allows us to gain more insight into why long-range travelling waves of activity may not develop in the impaired A1, regardless of the level of hearing loss.

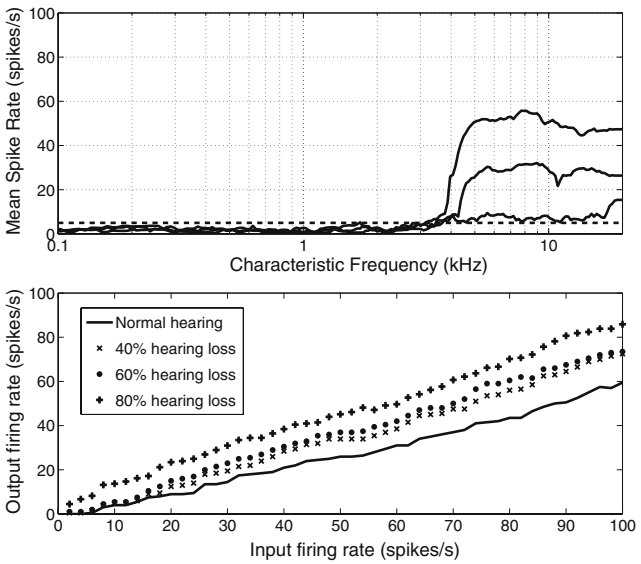

Fig. 4 Top panel: mean firing rates of the pyramidal neurons in response to spontaneous activity in the auditory thalamus (spike rate vs. characteristic frequency). Dashed curve: mean spike rate of the spontaneous input; Upper curve: model response after 80% hearing loss and HSP; Middle curve: model response after 60% hearing loss and HSP; Bottom curve: model response after 40% hearing loss and HSP. Bottom panel: input-output curves following HSP for different levels of hearing loss

Changes in spontaneous firing rates (SFR) induced by acoustic trauma have been studied in the auditory nerve fibers (where a drop in SFR is observed), dorsal cochlear nucleus (where an increase in SFR is observed), the inferior colliculus (where a drop in SFR is observed) and the A1 (where an increase in SFR is observed) (Basta et al. 2004; Eggermont and Roberts 2004). However, spontaneous firing rates in the auditory thalamus have not been sufficiently characterized. We modeled hearing loss in our thalamocortical inputs as an overall decrease in average firing rate based on firing rate changes in the inferior colliculus.

To investigate synchronous firing in the spontaneous activity of the A1 model, we compute the cross-correlation of the spike trains generated by different pyramidal neurons, using the following equation (Seki and Eggermont 2003; Noreña and Eggermont 2003):

$$p_{i,l}(d) = \frac{\left(\sum_t x_i(t)x_l(t-d) - N_i N_l/N\right)}{(N_i \cdot N_l)^{0.5}}, \tag{15}$$

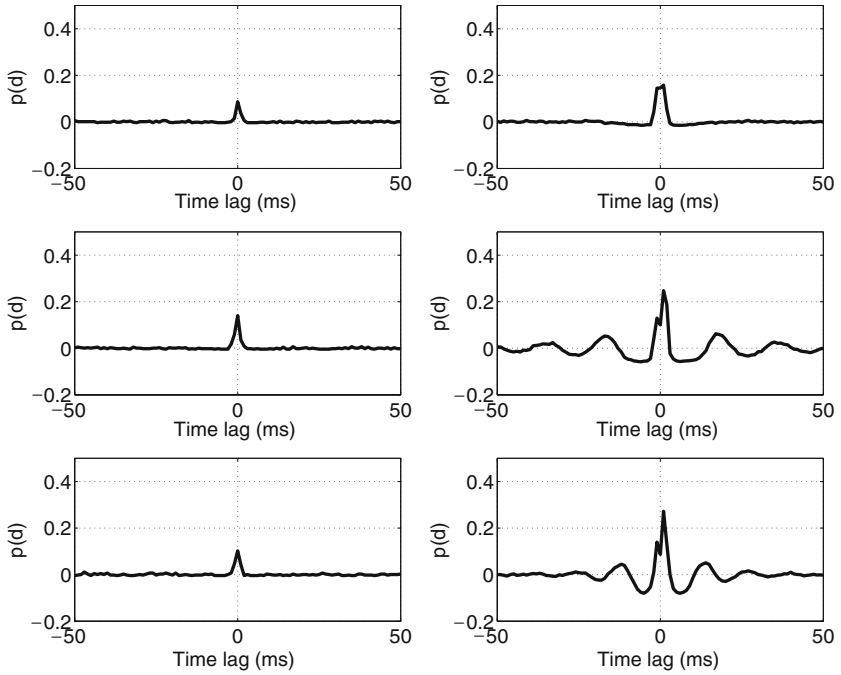

Fig. 5 Cross-correlation of the spontaneous activity of pyramidal neurons. The sub-figures in the first column present synchrony between the 51st pyramidal neuron (CF=380 Hz) and the 56th pyramidal neuron (CF=450 Hz), both of which are within the unimpaired region. The sub-figures in the second column show cross-correlation of firing activities between the 151st pyramidal neuron (CF=5.9 kHz) and the 156th pyramidal neuron (CF=6.6 kHz), both of which are within the impaired region. Results for different hearing loss levels are arranged in rows. The 1^{st} row: 40% hearing loss; the 2^{nd} row: 60% hearing loss; the 3^{rd} row: 80% hearing loss

where $x_i(t)$ and $x_l(t)$ represent the spike trains of the ith and the lth pyramidal neurons, respectively, d denotes the time lag spanning the range from −50ms to 50ms, N_i and N_l are the total number of spikes in $x_i(t)$ and $x_l(t)$, respectively, and N is the number of bins (bin size=2ms). In Fig. 5, we plot the cross-correlation as a function of the time lag d for two pairs of pyramidal neurons, one pair in the normal hearing region and the other pair in the impaired region. The neural synchrony between deafferentated excitatory neurons is significantly increased, compared with two normal neurons with the same spatial distance. Specifically, as shown in the figure, the peak value of the cross-correlation curve increases from approximately 0.1 to 0.17, 0.23, and 0.24 for 40%, 60% and 80% hearing loss levels, respectively. Although qualitatively similar, cross-correlation values obtained from simulations were an order of magnitude higher than those found in the literature (Seki and Eggermont 2002, 2003). This can be explained by the fact that our model of the auditory cortex contains significantly fewer neurons and connections (both lateral and afferent) than would be found in actual cortex. We developed a proof of concept model (not shown) with a variable number of inputs and outputs to demonstrate the effect of network connection complexity on peak cross-correlation values. As the number of input or output units in the network increased, the cross-correlation between any two output neurons decreased. Due to the computational complexity of a much larger network, we could not address this issue by scaling up our network.

In Fig. 6, we study the variations of the cross-correlation peaks as a function of the original characteristic frequencies of the pyramidal neurons. The peak value associated with each CF is determined by the maximum of the cross-correlation between the pyramidal neuron tuned to that CF under the condition of normal hearing (say, the ith neuron) and the other one

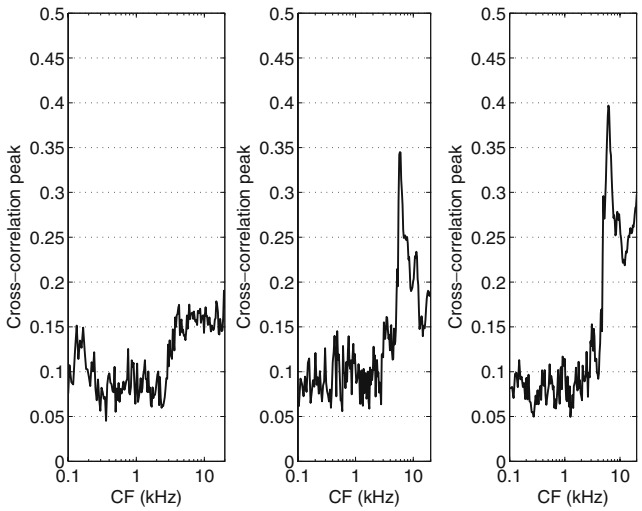

Fig. 6 The variation of cross-correlation peaks as a function of characteristic frequencies (CF). The peak value associated with each CF is the maximum of the cross-correlation between one pyramidal neuron with the same CF and another with spatial distance 6. Left sub-figure: peak variation curve after 40% hearing loss; Middle sub-figure: peak variation curve after 60% hearing loss; Right sub-figure: peak variation curve after 80% hearing loss

with spatial coordinate $i + 6$. From the figure, we can observe a clear elevation of the synchrony starting from the beginning of the hearing loss region at 2.5 kHz. Figure 6 shows that for higher levels of simulated hearing loss (60% and 80%), the greatest increase in synchrony occurs near the hearing-loss edge, where there is a stronger tendency for edge frequencies to drive these neurons. However, peak cross-correlation values are elevated across the hearing loss region. Thus, our model predicts that elevated synchrony in the hearing loss region may result from HSP-induced increased lateral excitation and decreased lateral inhibition; these are the same conditions that would be expected to produce travelling waves of activity.

3.2 Tuning properties after hearing loss

Since we are adjusting connection weights, it is important to look at potential changes in tuning. We do this by simulating a 50-ms input tone, varying its amplitude and center frequency, and observing the response of a neural unit in the hearing loss region. In Table 1, we look at potential changes in characteristic frequency and tuning sharpness for a unit with a normal CF of 5.2 kHz. We represent tuning sharpness using Q-values (Q20 in this case), which is analogous to what would be done for frequency-response-area plots obtained from electrophysiological recordings. Since our inputs are spikes at a certain rate rather than a sound level, Q20 is calculated by dividing the unit's CF by its bandwidth at an input rate 20 spikes/s above the minimum threshold. The minimum threshold is the lowest input tone rate required to elicit firing in the neuron; the center frequency of this tone is the unit's characteristic frequency. To determine the relevant bandwidth, the input tone's level is set to 20 spikes/s above the minimum threshold, and the lowest- and highest-frequency input tones that can elicit firing are determined. Tuning sharpness is reduced as the level of hearing loss increases; this is true for neural units throughout the hearing loss region. At 60% and 80% hearing loss, the Q20 value is substantially lower than in the normal scenario. Our model only shows small shifts in CF; they ranged from 0.05 octaves to 0.2 octaves in the neural units we looked at. In Table 1, we see a shift away from the hearing loss edge. Units closer to, or within, the sloping region of the hearing loss curve are more likely to exhibit CF-shifts to lower frequencies. On the other hand, units deeper in the hearing loss region could show CF-shifts towards higher or lower frequencies. This may be a result of the symmetry in our initial network connection weights. Namely, as the hearing loss curve is flat in these areas, the relative homeostatic adjustments may be stronger on one side of these units. The magnitude of weight adjustment could vary depending on the spontaneous inputs generated (using mutually independent Poisson processes) during homeostatic plasticity in our model. Furthermore, there may be an influence of the network edge at higher frequencies.

Table 1 Tuning properties of a neuron in the hearing loss region

Hearing loss level	Q20	Characteristic frequency (kHz)
No hearing loss	2.87	5.20
40% loss	2.40	5.76
60% loss	0.448	5.48*
80% loss	0.427	5.48*

This neural unit has a CF of 5.2 kHz when there is no hearing loss. At 60% and 80% hearing loss, there was no single frequency with the lowest threshold, so the one which evoked the strongest response is said to be the CF

While our homeostatic mechanism does not lead to significant tonotopic reorganization, it does have a substantial effect on tuning. Figure 7 compares changes in tuning for different levels of hearing loss in our model with tuning observed in a noise trauma experiment. To produce the rate-frequency-intensity contours we simulated 50-ms tones at frequencies from 1 kHz to 16 kHz and at levels from 10 to 65 spikes/s. We ran 5 simulations for each scenario and combined the responses. Noreña et al. (2003) presented each 15-ms tone pip 5 times at frequencies ranging from 625 Hz to 20 kHz. Our simulations show a broadening of the tuning curve with increased hearing loss. Furthermore, the CF becomes difficult to distinguish at 60% and 80% hearing loss levels. As in Table 1, it is evident that tuning becomes very broad for the higher levels of hearing loss in our model. We do not see threshold increases with hearing loss, and for this neural unit, a decrease in threshold is evident after 40% hearing loss. This may be due to too much compensation from our homeostatic mechanism and the lack of a realistic peripheral input model. The multi-unit activity (Noreña et al. 2003) after tonal trauma shows a variety of possible effects including a threshold decrease (see iii versus vii in Fig. 7(E)).

3.3 Sensitivity analysis

A sensitivity analysis demonstrates the impact of modifying key model parameters on two of our results: peak cross-correlation between two neural units and the spontaneous firing rate of a neural unit in the hearing loss region. Specifically, we look at the peak cross-correlation, in the region of simulated hearing loss, between neurons with characteristic frequencies

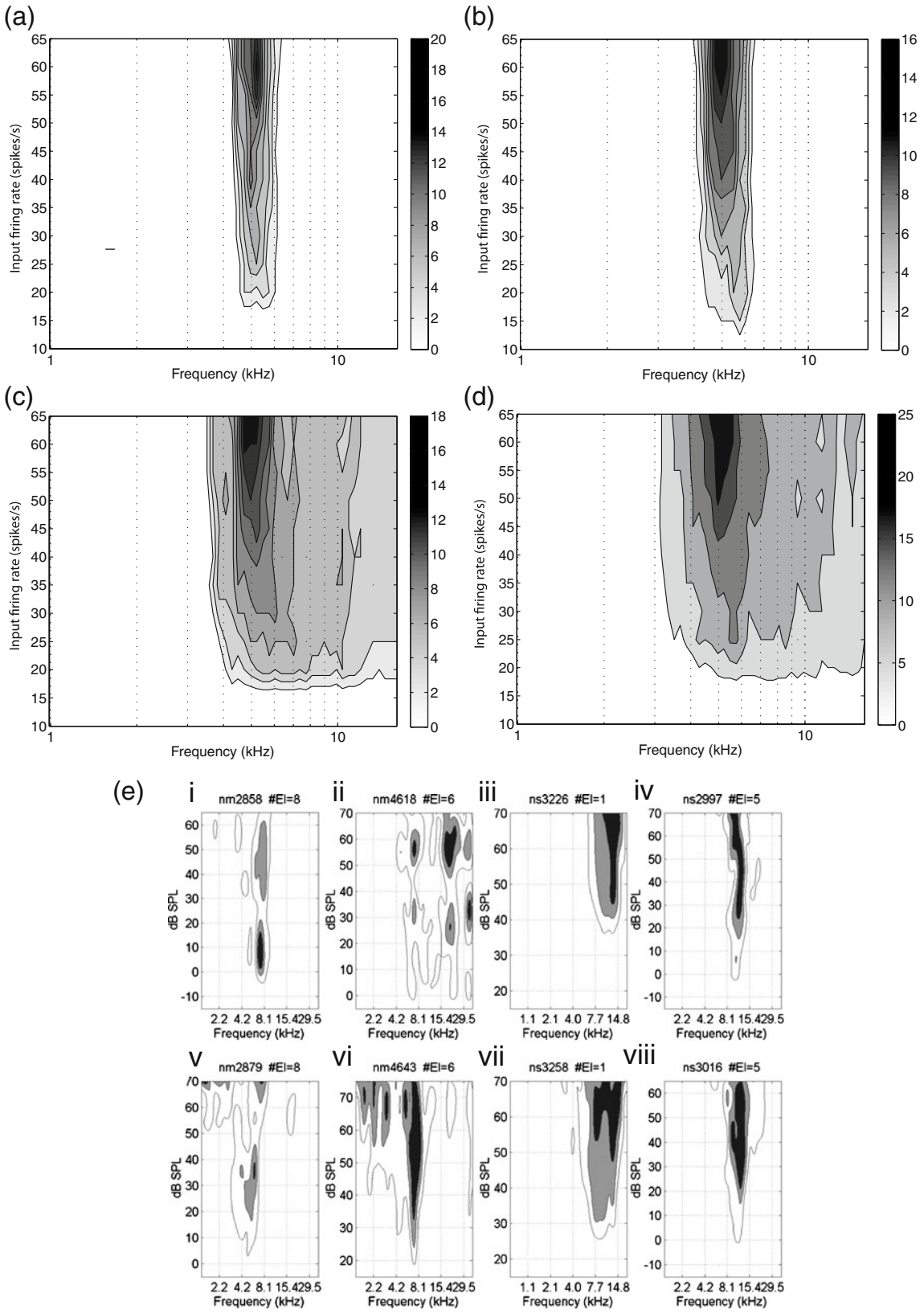

Fig. 7 Rate-frequency-intensity contours from our model and cat primary auditory cortex. The top portion of the figure shows simulated tuning curves from our model with no hearing loss (A), 40% (B), 60% (C) and 80% (D) hearing loss. Below (E), we include tuning curves from anesthetized cats before (top half) and after (bottom half) a 120 dB pure-tone trauma (Fig. 4 from Noreña et al. 2003)

Table 2 Sensitivity analysis

Parameter (*0.5:*2)	Peak cross-correlation	Spontaneous firing rate
Driving input rate	−0.7%:+22%	+34%:−27%
W_a initial	+67%:−37%	+52%:−14%
$W_{E,E}$ initial	−39%:+74%	+36%:−32%
$W_{I,E}$ initial	+12%:+4.3%	+5.3%:+3.9%
$W_{E,I}$ initial	−6.8%:+3.1%	−15%:22%

For each parameter, the value on the left and right side of the colon represents the change in the output metric after halving or doubling that parameter, respectively. The parameters we look at are: the driving rate in the simplified acoustic environment, the afferent connection weights, the connection weights between excitatory neurons, excitatory to inhibitory connection weights, and inhibitory to excitatory connection weights, respectively

5.2 kHz and 5.9 kHz (spatial distance of 6 neural units) and the spontaneous firing rate of the neural unit with a CF of 5.2 kHz. Table 2 lists changes in the output metrics when each parameter is halved or doubled. To reduce the number of required simulations, we choose one hearing loss condition (80% hearing loss) and modify the parameters for that scenario.

Increases in peak cross-correlation or spontaneous firing that result from changing parameters are acceptable since we expect these values to be elevated after hearing loss. The 37% and 39% decreases in peak cross-correlation that occur after doubling the initial afferent synaptic weights or halving the initial lateral excitatory weights, respectively, are still an order of magnitude lower than the increase in synchrony seen for 80% hearing loss (see Fig. 6). The same argument holds for the 27% and 32% reduction in spontaneous firing when the driving input rate during the homeostatic compensation is doubled or the initial connection weights between excitatory neurons are doubled, respectively (see top panel in Fig. 4).

3.4 Model prediction: spontaneous travelling waves

It is well known that travelling waves will appear in the rate-based Wilson-Cowan cortical model (Wilson and Cowan 1972, 1973; Wilson 1999) if the lateral inhibitory connections are weakened and excitatory connections are strengthened sufficiently (Wilson 1999; Wilson et al. 2001). Accordingly, we hypothesized that pyramidal neurons in our spiking A1 model (inspired by the Wilson-Cowan equations), might also generate travelling waves in the impaired region. Given that the amount of synaptic weight regulation is proportional to the hearing loss level, we predicted that travelling waves would be more likely for substantial hearing loss.

To test our hypothesis, we conducted the following simulations. The A1 models trained by HSP under different hearing loss scenarios are stimulated simultaneously by two pure tones with a duration of 15ms and input level of 50 spikes/s. We do not scale these

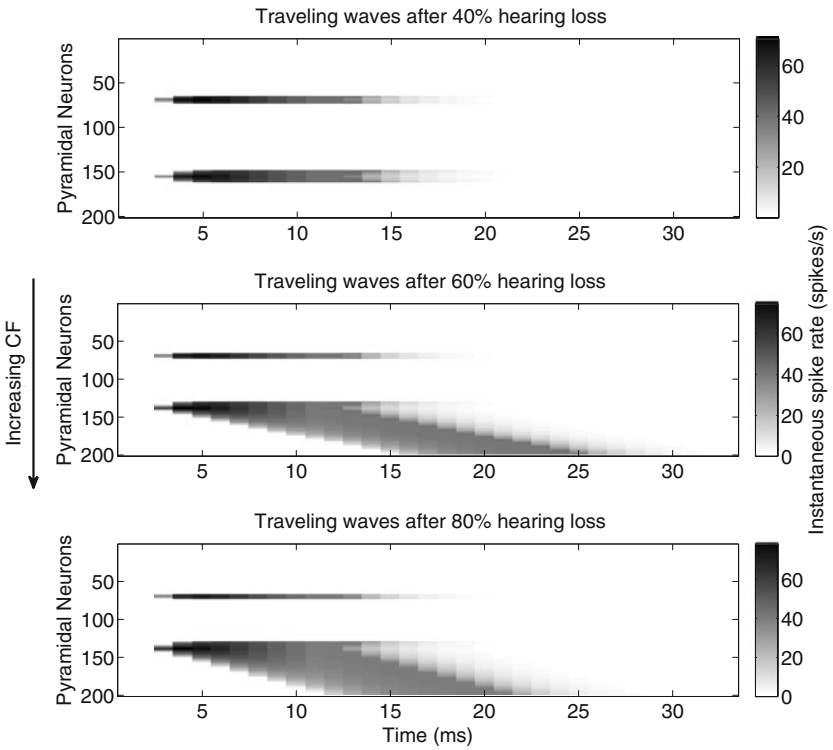

Fig. 8 Model responses to pure tones with no background spontaneous activity. For 40% hearing loss (top), the frequencies of the input pure tones are 723 Hz and 7.2 kHz. For 60% (middle) and 80% (bottom) hearing loss, the tonal stimuli have center frequencies of 723 Hz and 4.27 kHz. The bars beside the figures illustrate the intensity scale, where darker shades indicate higher stimulus-driven firing rates

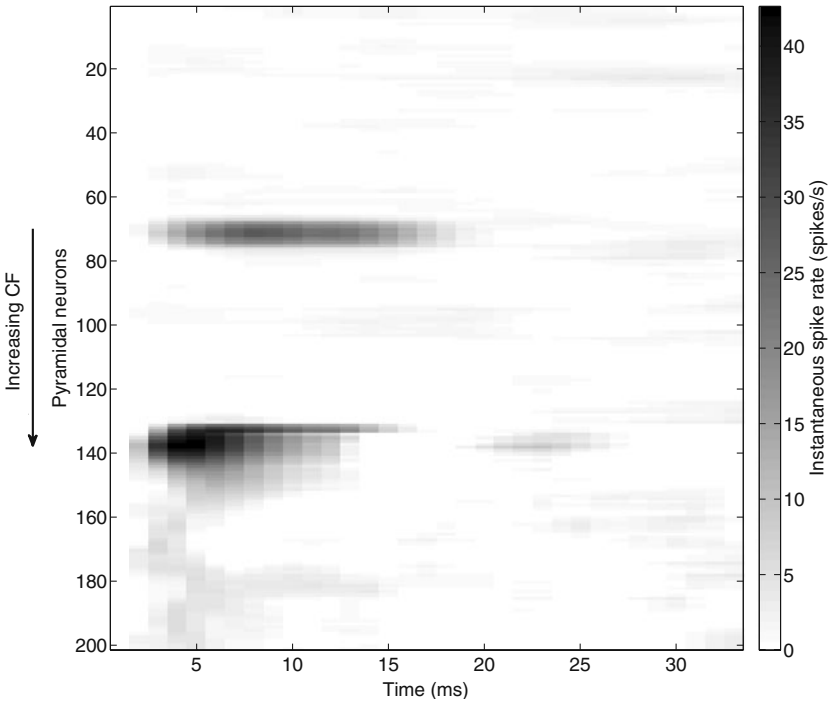

Fig. 9 The figure shows the lack of travelling waves when spontaneous firing is included in the input. The plot was created as follows: 100 trials of the 80% hearing loss scenario with input tones as described in Fig. 8 but with spontaneous firing included were averaged, 100 trials with only spontaneous firing were averaged, and finally, the latter average was subtracted from the former average

tones according to the level of hearing loss, as we have not described them as having the same sound level but rather, as inducing the same thalamic input rate. Scaling the tones according to the level of hearing loss does not qualitatively affect the results or existence of travelling waves discussed below. We first look at a case where there is no spontaneous firing, which is a scenario that is more analogous to the rate-based Wilson-Cowan cortical model.

The frequencies of the test tones are chosen so that one is within the normal region and the other is within the hearing loss region. The model responses to the

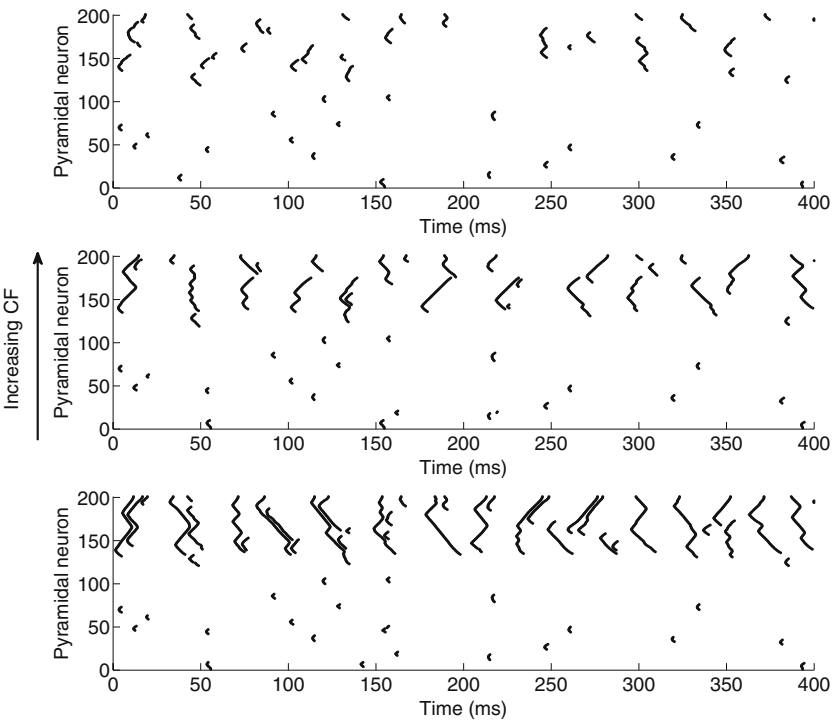

Fig. 10 Raster plots of spontaneous activity across the model A1 for different levels of hearing loss (deafferented region spans neurons 125–201). Top: 40%, middle: 60% and bottom: 80% all show increase in occurence and spatial extent of waves of excitation

tonal stimuli, quantitatively described by the instantaneous firing rates of the pyramidal neurons, were calculated using Eq. (12) with τ_r set to be 5ms. In the case of 60% and 80% hearing loss, pure tones at 723 Hz and 4.27 kHz are used, while for 40% hearing loss, pure tones at 723 Hz and 7.2 kHz are applied. For the 40% hearing loss scenario, the second tone was applied deeper in the impaired region to highlight that for this level of hearing loss, our model will not show tone-induced travelling waves. This is the case even though there is no spontaneous firing and the tone is applied in the region where lateral inhibitory connections are weakest. However, even at this level, spontaneous short-duration waves (shown in Fig. 10) occur. Thus, we establish that in our model, deafferentation above 40% is necessary to produce travelling waves of excitation when no spontaneous firing is present. In Fig. 3 we observe that the ratio of peak lateral inhibition on a pyramidal cell to peak lateral excitation drops to approximately 1 only at 60% hearing loss. This may be a necessary condition for the development of travelling waves when spontaneous firing is not present.

In Fig. 8, we plot the model responses in intensity maps of firing rates across spatial coordinates of the pyramidal neurons and time, in order to illustrate the propagation of the travelling waves in the case of no background spontaneous activity. After 60% and 80% hearing loss, a brief pure tone applied in the sloping region of the hearing loss curve caused sequential firing of the pyramidal neurons previously tuned to frequencies higher than the stimulus. In other words, a travelling wave appears; more importantly, with the travelling wave, all of the pyramidal neurons in the region of maximum hearing loss now become responsive to an edge frequency of the hearing loss spectrum (=4.27 kHz), which indicates the potential for cortical reorganization. This phenomenon can again be explained by the fact that HSP degrades inhibition and strengthens lateral excitation more for severe hearing loss. In contrast, after 40% hearing loss, even a tonal stimulus located within the most deafferentated region does not lead to propagating neural firing. Instead, compared with the model response to the 723-Hz pure tone in the normal hearing range, more neurons in the impaired region are excited by the input at 7.2 kHz. This phenomenon indicates the broadening of the tuning curves of the pyramidal neurons after hearing loss, which is consistent with experimental findings (Calford et al. 1993; Seki and Eggermont 2002; Noreña and Eggermont 2003).

As our model is based on a modified Wilson-Cowan cortical model, and travelling waves are clearly observed in this model for low levels of inhibition, it is expected that with a sufficient reduction in inhibition and increase in excitation, neural activity may propagate into neighboring neurons. Although we found that tonal stimulation in the deafferented region did produce long-range travelling waves with 60% and 80% hearing loss (Fig. 8), interestingly, this did not hold true when the model was also driven by inputs exhibiting spontaneous firing (5 spikes/s) (Fig. 9). This constitutes an unexpected finding by our model, as we are able to show that the types of long-range travelling waves predicted in a rate-based Wilson-Cowan cortical network will not necessarily occur in a spiking model with spontaneous firing inputs. Although we use a spontaneous input rate of 5 spikes/s, our simulations show that long-range travelling waves can be eliminated with spontaneous input rates as low as 1.5 spikes/s. It is also evident that even though travelling waves do not propagate across the hearing loss region, deafferented neurons do have less selective tuning.

A raster plot (Fig. 10) of activity during the silent condition, where the continuous driving rate is low, shows spontaneous waves of excitation with low temporal extent. We argue that with hearing loss, the rate of occurrence of waves of excitation increases, but their temporal extent is relatively unchanged because of interference from other waves of excitation. This lead to the hypothesis that while long-range travelling waves of excitation could be induced after hearing loss, interference by spontaneously evoked waves of excitation would severely limit their temporal extent. This could explain the lack of empirical evidence for long-range travelling waves of excitation in auditory cortex in spite of the presence of an increase in synchrony.

4 Discussion

We have presented a spiking model of primary auditory cortex (A1) and computational rules for the homeostatic regulation of synapses of different types, to address the question of whether travelling waves of neural activity could occur in A1 after hearing loss. The homeostatic plasticity (HSP) mechanisms were assumed to be the main driving force behind necessary changes to inhibition and excitation that would allow for travelling waves according to the Wilson-Cowan cortical equations. In addition, we postulated that homeostatic plasticity may be the neural mechanism underlying persistent abnormal neural activity in A1 observed after peripheral hearing loss. We showed through computer simulations that homeostatic

plasticity can scale synapses multiplicatively to bring the mean sound-driven firing rates of the deafferented cortical neurons back to a pre-specified target rate (i.e., the average firing rate of pyramidal neurons when stimulated by the same sound stimulus under the normal hearing condition). The compensatory effects of HSP lead to increased spontaneous activity and neural synchrony in impaired cortical regions, as has been found empirically (Seki and Eggermont 2003). These neural correlates of hearing loss in the auditory pathway, especially those in A1, are widely considered as potential substrates of tinnitus, the phantom sensation of a sound in the absence of any physical sound stimuli (Muhlnickel et al. 1998; Kaltenbach 2000; Eggermont 2003, 2005). Furthermore, our model shows an expansion of the excitatory response area for neurons in the hearing loss region. Calford et al. (1993) observed similar enlarged response areas in some neurons in A1 after tone-induced hearing loss. Unlike that study, we did not find contraction of any response areas or more complex changes. The reduced selectivity of the neural units in our model results from reduced lateral inhibition, which allows weaker thalamocortical inputs as well as cortico-cortical inputs to depolarize the neural unit above its threshold. Our simulations did not show tonotopic reorganization on the scale that has been described in studies of cochlear lesions (Robertson and Irvine 1989) and acoustic trauma (Seki and Eggermont 2002). The largest shifts we found were 0.2 octave shifts. Aside from peripheral and subcortical changes, there may be other mechanisms that we have not described in our model, which lead to tonotopic reorganization. Furthermore, they may operate on timescales that are greater than those in our analysis (Robertson and Irvine 1989). We observed shifts ranging from 0.05 to 0.2 octaves, with larger shifts occurring closer to the hearing-loss edge. These are certainly lower than shifts described by Robertson and Irvine (1989) (up to 0.625 octaves) after unilateral cochlear lesions and those (0.64–0.76 octaves) observed by Noreña et al. (2003) after pure-tone trauma. Near the edge of hearing loss, there are intact inputs from the normal hearing loss region that can shift the CF to lower frequencies. It should be pointed out that, our model sometimes showed an increase in CF, while most studies demonstrate a shift toward the frequencies of the lesion or noise trauma. We suggest that this may be the result of our network architecture: symmetrical connection weight distributions and perhaps network edge-effects at very high frequencies. Furthermore, this may imply that connections in our model do not span large enough distances, and so neural units that are not deafferented cannot sufficiently drive neurons deeper in the hearing loss region. Further evidence of this is the fact that greater shifts in CF occur closer to, and within, the sloping region of the hearing loss curve.

Hearing loss may also alter the inherent excitability of pyramidal neurons, which we did not include in our model. Kotak et al. (2005) found that sensorineural hearing loss can lead to a slightly depolarized resting membrane potential in pyramidal neurons of the auditory cortex. This may contribute to a higher spontaneous firing rate in these cortical neurons but does not necessarily explain an increase in synchrony of firing between cortical neurons. The elevated synchrony is better predicted by the strengthening of excitatory synapses on deafferented neurons (Vale et al. 2002; Muly et al. 2004; Kotak et al. 2005) and the weakening of inhibitory synapses onto these neurons (Suneja et al. 1998a, b; Vale et al. 2002; Kotak et al. 2005).

If homeostatic mechanisms enhance lateral excitatory and reduce lateral inhibitory connections, the Wilson-Cowan cortical model predicts travelling waves of neural activity. Our model indicates that travelling waves of activity are unlikely to develop in deafferented A1 when spontaneous activity is present. Rather, spontaneous, short-duration waves of excitation occur more frequently. The long-range travelling waves that are predicted by the Wilson-Cowan equations are prevented from spreading by these spontaneous short-duration waves. Specifically, it is the resultant refractory periods that prevent large-scale activity propagation in the network. Furthermore, the increased spontaneous firing that occurs in A1 after hearing loss would counteract network conditions that favor travelling waves because of the increase in spontaneous short-duration waves. Perhaps, as in the interactions of avalanches in models of running sandpiles (Hwa and Kardar 1992), the interactions of these spontaneous waves with each other and with any stimulus-induced wave, impede the observation of a single dominant travelling wave. However, the refractory period that follows the spontaneous short-duration waves, produces destructive interference, which differs from avalanche interaction and seems to be the main factor behind the lack of long-range travelling waves of activity.

While Fig. 8 clearly shows broadened tuning curves after the homeostatic modifications of connection weights, broadening of the tuning curves is also seen when spontaneous activity is introduced. Namely, Fig. 9 indicates that in the hearing loss region, neurons are less selective. Therefore, our model does not require conditions that allow for long-range travelling waves in order to demonstrate the broadening of tuning curves.

A recent model for epileptogenesis in isolated neocortex has produced results similar to the Wilson-Cowan equation predictions (Houweling et al. 2005). Using a network of Hodgkin-Huxley style neurons with both excitatory and inhibitory interactions, it was shown that HSP could lead to neural bursting and to waves travelling at 1.0–3.0 cm/s. A key difference between that model and the one we present here is that we apply HSP to a model of auditory cortex in which there was only partial deafferentation; this is more appropriate for hearing loss. In addition, deafferentation was restricted to the high frequency region of our model. Because of these differences we were able to show that only short-duration waves could span sections of the hearing loss region. As observed waves of excitation could develop throughout the impaired region, they may also play a role in cases of tinnitus where the percept is matched to frequencies spanning the hearing loss region (Eggermont and Roberts 2004). Furthermore, our simulation results (Fig. 10) imply that the short-duration waves may contribute to two changes in neural activity linked to tinnitus: increased spontaneous firing rates in deafferented neurons as well as increased synchrony between them and neurons they are connected to. Since neurons in the hearing loss region are less selective and allow for short-duration activity propagation, the spontaneous firing of each afferent will excite a greater number of cortical neurons, leading to greater spontaneous firing and synchrony. The similarity of our results to the results of Houweling et al. (2005) suggests that HSP may play a role in a range of cortical activity disorders including epilepsy and tinnitus. This has also been suggested in recent work by Fröhlich et al. (2008).

Several simpler computational models of the auditory system have addressed the role of HSP and related adaptation mechanisms to tinnitus. Schaette and Kempter (2006) proposed a single neuron model that qualitatively reproduces the hyperactivity observed in dorsal cochlear nucleus after increasing the synaptic gains of excitatory inputs. However, the choice of rate-based model neurons and lack of lateral connections in their model limits its ability to address the network-level changes in the temporal firing patterns such as neural synchrony. Dominguez et al. (2006) proposed a simple auditory cortical circuit model using spiking neurons, in which loss of auditory input was compensated for by enhancing the excitatory synapses and weakening inhibitory synapses on lateral connections. This model was able to capture enhanced synchrony in the deafferented region but was nonetheless limited in its ability to capture the full range of temporal dynamics, such as relative timing of excitatory and inhibitory responses. Our model builds on this work by 1) incorporating a computationally principled scheme for implementing HSP rather than manually adjusting the synaptic strengths, and 2) incorporating separate layers of excitatory and inhibitory neurons, so that more realistic temporal dynamics including travelling waves can be captured.

Finally, Fröhlich et al. (2008) use a computational network model of the neocortex to shed light on the development of dysfunctional cortical dynamics after deafferentation-induced homeostatic scaling of recurrent excitatory connections. This model predicted aberrant periodic bursting in the network if there was a critical level of deafferentation. We investigate the possibility of travelling waves by providing a more complete description of the changes in network dynamics through homeostatic plasticity. Namely, we propose formal computational mechanisms for HSP in both lateral and afferent connections. This addresses the lack of regulation of afferent connections and lateral connections onto inhibitory interneurons in the Fröhlich et al. (2008) model. In addition, while our homeostatic time constant is supported experimentally (Turrigiano et al. 1998), its update rate operates on the timescale of our simulated neural activity. This is not the case in the Fröhlich et al. (2008) model, where synaptic weights are updated at each 4-second interval.

One aspect of our model that is anatomically oversimplified is the manner by which we connect the input thalamic layer to the cortical layer to obtain relatively realistic tuning curves. It has been shown empirically that the functional convergence of thalamo-cortical projections spans about $\pm 1/3$ octaves (Miller et al. 2001), and we set the thalamo-cortical connections to match this functional convergence. However, it should be noted that auditory thalamic neurons can project to a much wider cortical region, while under normal hearing conditions, a large proportion of the excitatory synapses are functionally masked by thalamo-cortical input-driven inhibition. This feature is believed to provide the physiological basis for the rapid shifts in tuning curves, presumably due to unmasking of silent synapses, observed shortly after peripheral damage (Rajan 1998, 2001; Calford 2002; Noreña and Eggermont 2003). More specifically, it has been postulated that peripheral damage can reduce the stimulus-driven inhibition so that previously inhibited responsiveness can be unmasked. Our model developed in this paper has limited capability to fully account for the possible contributions of rapid unmasking to cortical changes observed shortly after cochlear impairment. Instead, we set up more constrained thalamo-cortical projections to separately investigate the potential role of HSP in inducing the cortical

abnormalities. It is possible that the acute cortical changes induced by unmasking effects, which might be weak at the beginning, are stabilized and strengthened by HSP so that they become detectable 2 hours after noise trauma (Noreña and Eggermont 2003) and persist in the following weeks (Seki and Eggermont 2003).

In the current version of our model, we did not include any Hebbian-like plasticity mechanism, such as spike timing dependent plasticity (Markram et al. 1997). This is largely because there is insufficient information on the characteristics of the output of the auditory thalamus. In our simulations with HSP, we assumed that the hearing-impaired model was exposed to a simplified acoustic environment where all the audible frequency components are mutually independent and possess the same average power over a large timescale. Under this assumption, correlation-based synaptic plasticity would not learn any pattern-specific features from the incoming acoustic stimuli, while HSP still functions. In future developments of the model, with the help of peripheral models such as the one developed by Zilany and Bruce (2006), we will combine pattern-specific learning with HSP.

Finally, the homeostatic response we simulate in response to hearing loss without including other factors or mechanisms may also compensate too well. If this is the case, it may reconcile the fact that in our model, tonal stimuli sometimes elicit stronger firing rates in the hearing loss region, even after their input rate is reduced according to the hearing loss level. Furthermore, this may help to explain why we do not see an elevated threshold after hearing loss in our model. Inclusion of a peripheral model that can incorporate cochlear hair cell impairment (such as that of Zilany and Bruce 2006) will allow more direct investigation of the effects of threshold elevation and other changes in peripheral tuning and excitability.

However, even with the above limitations, our model was able to produce a novel prediction with respect to travelling waves of neural activity in the deafferented A1. Using our comprehensive homeostatic mechanisms that scale different types of synapses, we were able to reproduce activity changes that are seen in animal models of sensorineural hearing loss. These alterations in spontaneous firing and neural synchrony resulted from homeostatic decreases of inhibition and increases of excitation in response to hearing loss. Furthermore, our model shows the broadening of tuning curves and some potential for slight tonotopic reorganization after hearing loss. While the Wilson-Cowan cortical model predicts long-range travelling waves under such conditions, by incorporating a greater level of biophysical detail including spiking neuronal dynamics and spontaneous activity, we refine this prediction; it is postulated that short-duration travelling waves of a more limited spatial extent could be observed in animal models of hearing impairment and tinnitus. Our findings on spontaneous short-range waves of excitation provide new insight into potential mechanisms underlying tonotopic remapping after deafferentation that will be explored in future work.

Acknowledgements The authors would like to express their gratitude to the reviewers for important feedback and advice, and to Dr. Jos J. Eggermont for his critical comments on earlier versions of this manuscript.

References

Basta, D., & Ernest, A. (2004). Noise-induced changes of neuronal spontaneous activity in mice inferior colliculus brain slices. *Neuroscience Letters, 368*, 297–302.

Bhattacharyya, T., & Dayal, V. (1989). Influence of age on hair cell loss in the rabbit cochlea. *Hearing Research, 40*, 179–183.

Brozoski, T., Bauer, C., & Caspary, D. (2002). Elevated fusiform cell activity in the dorsal cochlear nucleus of chinchillas with psychophysical evidence of tinnitus. *Journal of Neuroscience, 22*, 2383–2390.

Bruce, I., Bajaj, H., & Ko, J. (2003). Lateral-inhibitory-network models of tinnuts. In *Proceedings of the 5th IFAC symposium on modeling and control in biomedical systems* (pp. 359–363). Dordrecht: Elsevier.

Burrone, J., & Murthy, V. (2003). Synaptic gain control and homeostasis. *Current Opinion in Neurobiology, 13*, 560–567.

Calford, M. (2002). Dynamic representational plasticity in sensory cortex. *Neuroscience, 111*, 709-738.

Calford, M., Rajan, R., & Irvine, D. R. F. (1993). Rapid changes in the frequency tuning of neurons in cat aduitory cortex resulting from pure-tone-induced temporary threshold shift. *Neuroscience, 55*(4), 953-964.

Charles, A. & Brennan, K. (2009). Cortical spreading depression-new insights and persistent questions. *Cephalagia, 29*(10), 1115–1124.

Chen, Q., & Jen, P. (2000). Bicuculline application affects discharge patterns, rate-intensity functions, and frequency tuning characteristics of bat auditory cortical neurons. *Hearing Research, 150*, 161–174.

Cheung, S., Bedenbaugh, P., Nagarajan, S., & Schreiner, C. (2001). Functional organization of squirrel monkey primary auditory cortex: Responses to pure tones. *Journal of Neurophysiology, 85*, 1732–1749.

Dayan, P., & Abbott, L. F. (2005). *Theoretical neuroscience: Computational and mathematical modeling of neural systems*. The MIT Press.

Desai, N., Cudmore, R., Nelson, S., & Turrigiano, G. (2002). Critical periods for experience-dependent synaptic scaling in visual cortex. *Nature Neuroscience, 5*, 783–789.

Dietrich, V., Nieschalk, M., Stoll, W., Rajan, R., & Pantev, C. (2001). Cortical reorganization in patients with high frequency cochlear hearing loss. *Hearing Research, 158*, 95–101.

Dominguez, M., Becker, S., Bruce, I., & Read, H. (2006). A spiking neuron model of cortical correlates of sensorineural hearing loss: Spontaneous firing, synchrony and tinnitus. *Neural computation, 18*(12), 2942–2958.

Douglas, R., & Martin, K. (1998). Neocortex. In G. M. Shepherd (Ed.), *The synaptic organization of the brain* (pp. 459–509). New York: Oxford University Press.

Eggermont, J. (2000). Sound induced correlation of neural activity between and within three auditory cortical areas. *Journal of Neurophysiology, 83*, 2708–2722.

Eggermont, J. (2003). Central Tinnitus. *Auris Nass Larynx, 30*, 7–12.

Eggermont, J. (2005). Tinnitus: Neurobiological substrates. *Drug Discovery Today 19*, 1283–1290.

Eggermont, J., & Roberts L. E. (2004). The neuroscience of Tinnitus. *Trends in Neurosciences, 27*, 676–682.

Foeller, E., Vater, M., & Kossl, M. (2001). Laminar analysis of inhibition in the gerbil primary auditory cortex. *Journal of the Association for Research in Otolaryngology, 2*(3), 279–296.

Fröhlich, F., Bazhenow, M., & Sejnowski, T. (2008). Pathological effect of homeostatic synaptic scaling on network dynamics in diseases of the cortex. *Journal of Neuroscience, 28*(7), 1709–1720.

Gerken, G. (1996). Central tinnitus and lateral inhibition: An auditory brainstem model. *Hearing Research, 97*, 75–83.

Gestner, W., & Kistler, W. (2002). *Spiking neuron models: Single neurons, populations, plasticity*. Cambridge University Press.

Greenwood, D. (1990). A cochlear frequency-position function for several species-29 years later. *Journal of the Acoustical Society of America, 87*, 2592–2605.

Houweling, A., Bazhenov, M., Timofeev, I., Steriade, M., & Sejnowski, T. (2005). Homeostatic synaptic plasticity can explain post-traumatic epileptogenesis in chronically isolated neocortex. *Cerebral Cortex, 15*, 834–845.

Hwa, T., & Kardar, M. (1992). Avalanches, hydrodynamics, and discharge events in models of sandpiles. *Physical Review A, 45*, 7002–7023.

Jones, E. (1995). Overview: Basic elements of the cortical network. In M. J. Gutnick & I. Moody (Ed.), *The Cortical Neuron* (pp. 111–122). New York: Oxford University Press.

Kaltenbach, J. (2000). Neurophysiologic mechanisms of Tinnitus. *Journal of the American Academy of Audiology, 11*, 125–137.

Kaltenbach, J., Zacharek, M., Zhang, J., & Frederick, S. (2004). Activity in the dorsal cochlear nucleus of hamsters previously tested for tinnitus following intense tone exposure. *Neuroscience Letters, 355*, 121–125.

Kilman, V., van Rossum, M., & Turrigiano, G. (2002). Activity deprivation reduces miniature IPSC amplitude by decreasing the number of postsynaptic GABA(A) receptors clustered at neocortical synapses. *Journal of Neuroscience, 22*, 1328–1337.

Komiya, H., & Eggermont, J. (2000). Spontaneous firing activity of cortical neurons in adult cats with reorganized tonotopic map following pure-tone trauma. *Acta Otorhinolaryngologica, 120*, 750–756.

Konig, O., Schaette, R., Kempter, R., & Gross, M. (2006). Course of hearing loss and occurrence of tinnitus. *Hearing Research, 221*, 59–64.

Kotak, V., Fujisawa, S., Lee, F., Aoki, C., & Sanes D. (2005). Hearing loss raises excitability in the auditory cortex. *Journal of Neuroscience, 25*, 3908–3918.

Liberman, M. (1987). Chronic ultrastructural changes in acoustic trauma: Serial-section reconstruction of stereocilia and cuticular plates. *Hearing Research, 26*, 65–88.

Leslie, K., Nelson, S., & Turrigiano, G. (2001). Postsynaptic depolarization scales quantal amplitude in cortical pyramidal neurons. *Journal of Neuroscience, 21*, 1–6.

Lu, Y., & Jen, P. (2001). GABAergic and glycinergic neural inhibition in excitatory frequency tuning of bat inferior collicular neurons. *Experimental Brain Research, 141*, 331–339.

Markram, H., Lubke, J., Frotscher, M., & Sakmann, B. (1997). Regulation of synaptic efficacy by coincidence of postsynaptic APs and EPSPs. *Science, 275*, 213–215.

Merzenich, M., Knight, P., & Roth, G. (1975). Representation of cochlea within primary auditory cortex in the cat. *Journal of Neuroscience, 38*, 231–249.

Miller, L., Escabi, M., Read, H., & Schreiner, C. (2001). Functional convergence of response properties in the auditory thalamocortical system. *Neuron, 32*, 151–160.

Milner, P. M. (1958). Note on a possible correspondence between the scotomas of migraine and spreading depression of Leao. *Electroencephalography and Clinical Neurophysiology, 10*, 705.

Muhlnickel, W., Elbert, T., Taub, E., & Flor, H. (1998). Reorganization of auditory cortex in tinnitus. *Proceedings of the National Academy of Sciences, 95*, 10340–10343.

Muly, S., Gross, J., & Potashner, S. (2004). Noise trauma alters D-[3H]aspartate release and AMPA binding in chinchilla cochlear nucleus. *Journal of Neuroscience Research, 75*, 585–596.

Noreña, A. & Eggermont, J. (2003). Changes in spontaneous neural activity immediately after an acoustic trauma: Implications for neural correlates of tinnitus. *Hearing Research, 183*, 137–153.

Noreña, A., Tomita M., & Eggermont, J. (2003). Neural changes in cat auditory cortex after a transient pure-tone trauma. *Journal of Neurophysiology, 90*, 2387–2401.

Ottaviani, F., Di Girolamo, S., Briglia, G., De Rossi, G., Di Giuda, D., & Di Nardo, W. (1997). Tonotopic organization of human auditory cortex analyzed by SPET. *Audiology, 36*, 241–248.

Parra, L. C. & Pearlmutter, B. A. (2007). Illusory percepts from auditory adaptation. *Journal of the Acoustical Society of America, 121*, 1632–1641.

Phillips, D., & Irvine, D. (1981). Responses of single neurons in physiologically defined primary auditory cortex AI of the cat: Frequency tuning and responses to intensity. *Journal of Neurophysiology, 45*, 48–58.

Popelar, J., Erre, J., Aran, J., & Cazals, Y. (1994). Plastic changes in ipsicontralateral differences of auditory cortex and inferior colliculus evoked potentials after injury to one ear in the adult guinea pig. *Hearing Research, 72*, 125–134.

Rajan, R. (1998). Receptor organ damage causes loss of cortical surround inhibition without topographic map plasticity. *Nature Neuroscience, 1*, 138–143.

Rajan, R. (2001). Plasticity of excitation and inhibition in the receptive field of primary auditory cortical neurons after limited receptor organ damage. *Cerebral Cortex, 11*, 171–182.

Rajan, R., Irvine, R., Wise, L., & Heil, P. (1993). Effect of unilateral partial cochlear lesions in adult cats on the representation of lesioned and unlesioned cochleas in primary auditory cortex. *Journal of Comparative Neurology, 338*, 17–49.

Read, H., Winer, J., & Schreiner, C. (2002). Functional architecture of the auditory cortex. *Current Opinion in Neurobiology, 12*, 433–440.

Riegle, K., & Meyer, R. (2007). Rapid homeostatic plasticity in the intact adult visual system. *Journal of Neuroscience, 27*, 10556–10567.

Robertson, D., & Irvine, D. R. F. (1989). Plasticity of frequency organization in auditory cortex of guinea pigs with partial

unilateral deafness. *Journal of Comparative Neurology*, 282, 456–471.

van Rossum, M., Bi, G., & Turrigiano, G. (2000). Stable Hebbian learning from spike-timing dependent plasticity. *Journal of Neuroscience, 20*, 8812–8821.

Rutherford, L., Dewan, A., Lauer, H., & Turrigiano G. (1997). Brain-deprived neutrotrophic factor mediates the activity-dependent regulation of inhibition in neocortical cultures. *Journal of Neuroscience, 17*, 4527–4535.

Rutherford, L., Nelson, S., & Turrigiano, G. (1998). Opposite effects of BDNF on the quantal amplitude of pyramidal and interneuron excitatory synapses. *Neuron, 21*, 521–530.

Salvi, R., Henderson, D., Hamernik, R., & Parkins, C. (1980). VIII nerve response to click stimuli in normal and pathological cochleas. *Hearing Research, 2*, 335–342.

Salvi, R., Wang, J., & Ding, D. (2000). Auditory plasticity and hyperactivity following cochlear damage. *Hearing Research*, 147, 261–274.

Schaette, R., & Kempter, R. (2006). Development of tinnitus-related neuronal hyperactivity through homeostatic plasticity after hearing loss: a computational model. *European Journal of Neuroscience, 23*, 3124–3138.

Schreiner, C., Read, H., & Sutter, M. (2000). Modular organization of frequency integration in primary auditory cortex. *Annual Review of Neuroscience, 23*, 501–529.

Seki, S., & Eggermont, J. (2002). Changes in cat primary auditory cortex after minor-to-moderate pure-tone induced hearing loss. *Hearing Research, 173*, 172–186.

Seki, S., & Eggermont, J. (2003). Changes in spontaneous activity firing rate and neural synchrony in cat primary auditory cortex after localized tone-induced hearing loss. *Hearing Research, 180*, 28–38.

Suneja, S., Benson, C., & Potashner, S. (1998a). Glycine receptors in adult guinea pig brain stem auditory nuclei: Regulation after unilateral cochlear ablation. *Experimental Neurology, 154*, 473–488.

Suneja, S., Potashner, S., & Benson, C. (1998b). Plastic changes in glycine and GABA release and uptake in adult brain stem auditory nuclei after unilateral middle ear ossicle removal and cochlear ablation. *Experimental Neurology, 151*, 273–288.

Takano, T., Tian, G. F., Peng, W., Lou, N., Lovatt, D., Hansen, A. J., et al. (2007). Cortical spreading depression causes and coincides with tissue hypoxia. *Nature Neuroscience, 10*(6), 754–762.

Turner, J., Hughes, L., & Caspary, D. (2005). Divergent response properties of layer-V neurons in rat primary auditory cortex. *Hearing Research, 202*, 129–140.

Turrigiano, G., Leslie, K., Desai, N., Rutherford, L., & Nelson, S. (1998). Activity dependent scaling of quantal amplitude in neocortical pyamidal neurons. *Nature, 391*, 892–895.

Vale, C., & Sanes, D. (2002). The effect of bilateral deafness on excitatory and inhibitory synaptic strength in the inferior colliculus. *European Journal of Neuroscience*, 16, 2394–2404.

Wang, J., Salvi, R., & Powers, N. (1996). Plasticity of response properties of inferior colliculus neurons following acute cochlear damage. *Journal of Neurophysiology, 75*, 171–183.

Wang, J., Ding, D., & Salvi, R. (2002). Functional reorganization in chinchilla inferior colliculus associated with chronic and cochlear damage. *Hearing Research, 168*, 238–249.

Wehr and Zador (2003). Balanced inhibition underlies tuning and sharpens spike timing in auditory cortex. *Nature, 426*, 442–446.

Wilson, H. (1999). *Spikes, decisions and actions: dyanmic foundations of neuroscience*. Oxford University Press.

Wilson, H., & Cowan, J. (1972). Excitatory and inhibitory interactions in localized populations of model neurons. *Biophysical Journal, 12*, 1–24.

Wilson, H., & Cowan, J. (1973). A mathematical theory of the functional dynamics of cortical and thalamic nervous tissue. *Kybernetics, 13*, 55–80.

Wilson, H., Blake, R., & Lee, S. (2001). Dynamics of travelling waves in visual perception. *Nature, 412*, 907–910.

Zilany, M., & Bruce, I. (2006). Modeling auditory-nerve responses for high sound pressure levels in the normal and impaired auditory periphery. *Journal of the Acoustical Society of America, 120*, 1446–1466.